Report 7, 1990

GRAVITY AND MAGNETIC ASSESSMENT OF THE TENORIO AREA, COSTA RICA

Dagoberto Herrera Cabezas,
UNU Geothermal Training Programme,
Orkustofnun - National Energy Authority,
Grensásvegur 9,
108 Reykjavik,
ICELAND

Permanent address:
Instituto Costarricense de Electricidad,
Recursos Geotérmicos,
Apdo 10032-1000,
San José,
COSTA RICA

ABSTRACT

The Tenorio area is located about 20 km from the Miravalles geothermal field which is a high temperature productive geothermal area, and is related to a major volcanic system referred to as the Tenorio volcano. This report partially represents the terminal stage of the pre-feasibility study done in 1989. It deals with the analysis of gravity and ground magnetic data over 550 km^2. The study starts with the density determination, followed by an anomaly separation from a statistically determined regional trend surface and ends with a frequency analysis of the Bouguer anomaly thus obtained. The analysis is carried out by means of directional filtering and frequency filtering, enhancing or removing linear features, and enhancing or removing spatial frequency ranges.

The potential methods can be referred to as structural methods, regarding them as an extension of the geological mapping. Therefore, a structural synthesis map with the structures suggested in this report and the ones found previously by other means, is offered and briefly discussed within a geothermal context. A mass estimation of one of the larger anomalies is also offered. Two main fault systems are proposed: 1) A NW-SE system correlated with the oldest system whose signature seems to be traceable all over the southern part of the area; 2) An almost perpendicular NE-SW system, apparently much more recent, forming a pattern of blocks confined by these and the previous set of faults. A caldera border is extended after the analysis of the gravity map low-pass filtering. A negative magnetic belt is considered with a NE-SW strike overcoming the anomalies of the south. A possible association of gravity highs with magnetic lows is suggested.

TABLE OF CONTENTS

LIST OF FIGURES

LIST OF TABLES

1. INTRODUCTION

1.1 Aim of the study and the Tenorio area

Between November 1987 and October 1988 a national evaluation of geothermal resources was carried out in Costa Rica by the ICE (Instituto Costarricense de Electricidad) to select prospective areas suitable for a more detailed stage of exploration. As a result two volcanic zones besides the Miravalles Geothermal field were chosen as high priority areas for further study, namely the volcanoes of Rincón de La Vieja and Tenorio.

Since 1989, the Tenorio volcano area has been under a pre-feasibility study to determine its geothermal potential. Studies such as geochemical analysis of surface waters and gas samples, plus resistivity profiling, magnetotellurics, gravity and ground magnetic surveys were carried out.

This report was proposed as a research project, in fulfilment of the specialized training given by the United Nations University Geothermal Training Programme in Iceland; the work deals with the processing and interpretation of gravity and magnetic data in the Tenorio area.

The survey area is situated in a volcanic range, characterized by the occurrence of paired volcanoes, that crosses the country from northwest to southeast, almost to latitude 10°N in the central part of the country. It is located at the base of the Tenorio-Montezuma volcanic system that runs NNE-SSW and is surrounded by circular segments that suggest large sinking areas (caldera structures).

The region is characterized by intense volcanic activity since the early Pleistocene, although evolutionary products suggesting a resident time accounting for its differentiation have also been found. These, together with volcano-tectonic collapses, strongly suggest a shallow magmatic system not manifested in recent time, but revealed by hydrothermal activity and thermal gradients as high as 18°C/100 m.

The stratigraphy consists of alternate layers of lavas and pyroclastic rocks, with a thickness of a few hundred meters, overlying a basement which is essentially composed of andesite and basaltic lavas which may constitute the reservoir. The permeability of this sequence is mainly controlled by secondary alteration, which presumably constitutes the caprock of the potential geothermal system. Above this caprock, the meteoric water infiltrates and masks the possible deep-seated thermal anomaly.

The linear structural trends observed are mainly grabens that run NW-SE towards the southeast of the area and N-S towards the northwest. The major structures recognized are: the Arenal graben that ends against a small structure perpendicular to the Sn. Lorenzo river, and the Bijagua graben inferred by the resistivity surveys, although not confirmed in this report.

This general geological information leads to the consideration of two anomalous temperature areas, based on evidence of hydrothermal activity and structural context: one in the surroundings of the Sn. Lorenzo river, and the other near the Celeste river; the first one was chosen as a priority exploration target for a high temperature system.

1.2 Previous research

In the first stage of exploration 452 gravity measurements and 511 ground magnetics

measurements were taken, with a mean density of one station per square kilometre, covering an area of about 550 km^2. Rock samples for density and susceptibility determinations were taken from surface rocks and from boreholes; a total of 97 density and 82 magnetic susceptibility measurements were made.

The gravity data used in this report was originally reduced to the Bouguer anomaly using 2300 kilograms per cubic meter. The ground magnetic data obtained simultaneously was corrected for the diurnal variations using IGRF and refers to the first station when the survey began. The result of this preliminary work is shown on the geological map (Figure 1) as a structural and geological synthesis.

This study will start with density determination. The density is selected by several standard methods and the results compared, with a brief discussion of the methods and their results. Once the data has been reduced to the Bouguer anomaly, we will try to separate the anomalies from regional features, modelling the local deviations qualitatively. The anomaly separation techniques include both an ANOVA analysis of polynomials fitted to the data in the least squares sense and spectral analysis using the FFT algorithm. The main task of this work is to provide some detail in the priority areas where we have more information, i.e. the Sn. Lorenzo and Celeste rivers, and practice some modelling with mass determination. Also of interest is to make a clear correlation between the gravity and magnetic maps.

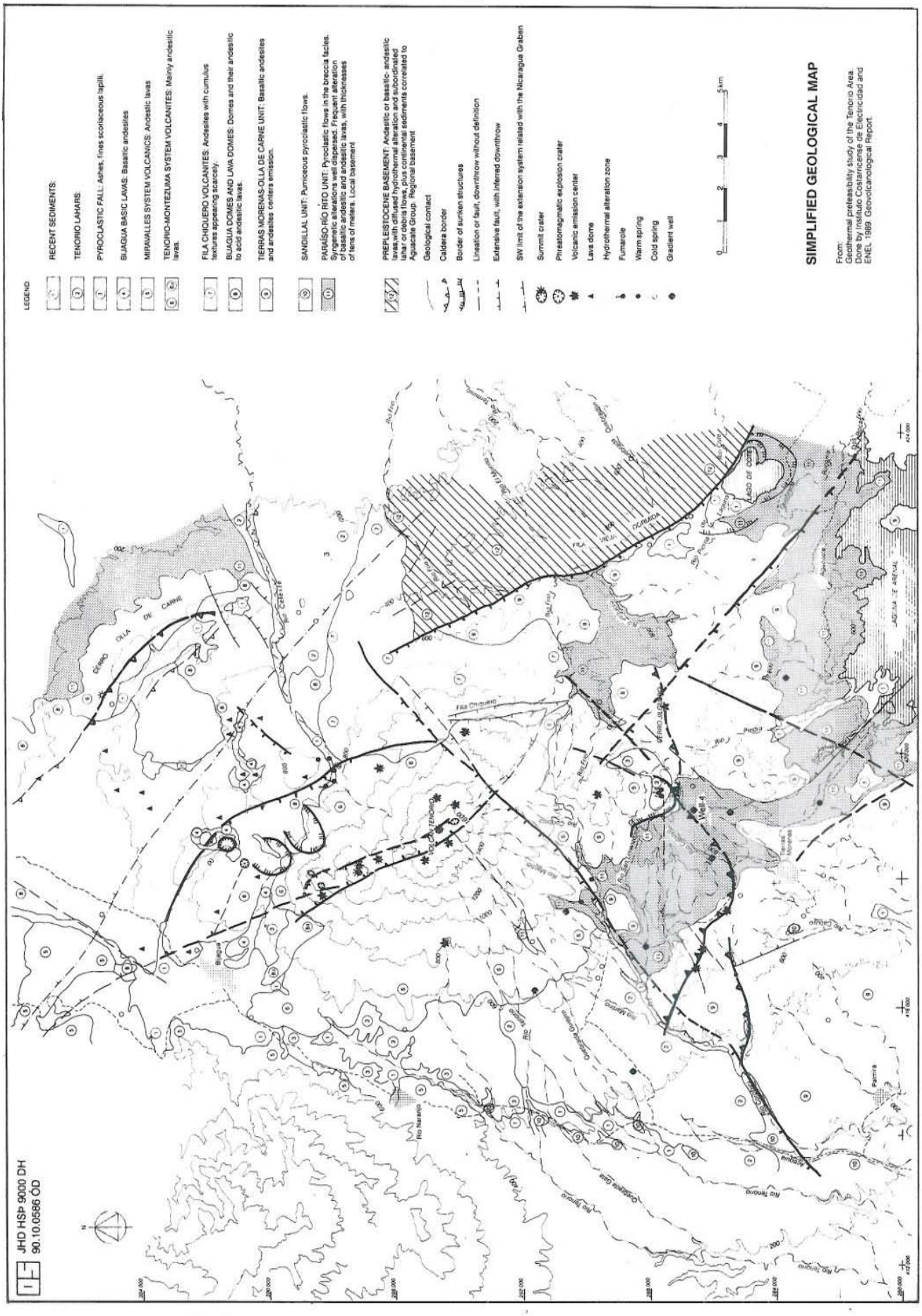

FIGURE 1: Simplified geological map of the Tenorio area

2. GEOLOGY

The majority of the rocks are volcanites with lavas of intermediate composition and limited extension, determined mainly by their centres of emission. The thickness is, therefore, highly variable. Only two rock formations differ from this general composition: the first one is constituted by the volcanic rocks from the pre-Pleistocene which constitutes the deeper regional basement extending throughout the area, and the Paraíso-Río Rito units and their distal facies Sandillal unit, composed mainly of pyroclastic flows alternating with lavas, with maximum thicknesses of about 300 m that form the local basement. It is supposed that these two were deposited in sequence.

The area is characterized by almost vertical normal faulting and the predominant directions are NW-SE and NE-SW. In these systems are included sinking structures, several kilometres wide, with displacements of a few tens of meters. Two exceptions are Fila Dormida to the west and Fila Chiquero towards the centre (Figure 1) where expected displacements are hundreds of meters. The structural trend of the area can be traced out as a series of elongated blocks NNW-SSE cut by much smaller transversal lineaments with NE-SW direction. It is noteworthy that a NW-SE regional pattern might be inferred from the migration of volcanic centres as was mentioned in the introduction. Almost all the rocks are strongly affected by neo-tectonic alignments. The more intense fracturing occurs between the northwest end of the Arenal graben and the Tenorio volcano. The Sn. Lorenzo river is probably associated with the outermost northwest side of the graben, coinciding with the appearance of semicircular sinking structures and fossil alteration activity in the vicinity (Figure 1). Río Celeste is very likely related to the extension of the Chiquero range fault.

During the Miocene, many calc-alkaline products were deposited with outcropping thicknesses of andesitic lavas piles of about 800-1000 meters. These lavas are considered to be the pre-Pleistocene basement, known as the Aguacate Group which only outcrops to the east of the geological map (Figure 1, lithological unit 12). In the early Pliocene the tectonism had a preferential WNW-ESE strike. The major structure is the Arenal graben, which may be related to the same tectonic cycle as the Nicaragua graben.

In the early Pleistocene there was prominent explosive activity where the Tenorio volcano now is, with emissions of pyroclastic flows. These were bounded by the northeast flank of the Arenal graben. Probably at the same time, and especially at the centre, lava emissions in large volumes (tens of cubic kilometres) occurred producing circular structures resembling calderas. The subsequent activity centralized at the borders of the "caldera structures", giving rise to volcanic edifices (Olla de Carne to the northeast, Bambú, etc.) whose products were deposited mainly towards the south (Tierras Morenas plateau).

In the early to late Pleistocene the activity occurred mainly in the inner part of the caldera but was very scattered as can be seen from the distribution of volcanic edifices. Domes and lava domes in the northern area, referred to as Bijagua lavas on the geological map, were extruded. At the same time, the predominant WNW-ESE strike changed to NNW-SSE, preserving its extensional characteristics.

A strato-volcano was built up around the centre in the late Pleistocene. Later, its eastern flank collapsed (Fila chiquero) forming a suitable place for the occurrence of another volcanic cycle with new NNW-SSE faulting directions, giving rise to the recent edifices of the Tenorio system. Intensive neo-tectonism is associated with this stage in the NNW-SSE direction, confirmed by the following volcanic edifices and by a large NE-SW fault towards the southwest.

3. DATA PROCESSING

The Bouguer anomaly map is the end result of the gravimetric field work, obtained by using Hammer's terrain correction up to 5 km, and up to 20 km by using a modification of Hammer. The density used in this original reduction was 2.3 g/cm^3, derived from the reduction density used in the Miravalles geothermal field, which was the model used as a paradigm for the first approach to neighbouring fields.

A quick look at the gravity map suggests some of the structures that were verified, but others were added as will be described later in the results. The Bouguer anomalies vary from -25.5 to 5.8 milligals with two maximums, not very well defined, as they are located near the borders of the surveying area. Two sharp NW-SE gradient belts are shown practically parallel to the Tenorio river. These two belts constrain a deficiency in mass, separating two major volcanic complexes, the Tenorio volcano and the Miravalles volcano. A geothermal project is currently in the developmental stage at Miravalles.

It is important to keep in mind the magnitude of the gravity field. Only 0.3% of the total field comes from the crust, and 0.005% comes from the uppermost five kilometres. As the anomalies of our analysis probably do not exceed 0.01 of this value, in order to be effective one must be cautious in evaluating the sensitivity of the instrumentation to perceive these changes and the methods used to compensate the measurements that will certainly influence any further data treatment.

3.1 Best density choice

The first parameter considered in preparing the gravity data for interpretation is the density of the rocks above the Bouguer reference level. The density of the topographic masses needs to be known for the Bouguer and terrain correction computations, otherwise these lead to fictitious anomalies and corresponding misinterpretations. But at the same time, it is clear that the inverse problem of gravimetry such as the computation of the density function (location and form of the disturbing masses, as well as the density) is very difficult to assess without other geological or geophysical information.

It is important to choose a bulk density distribution which reflects a least possible relationship with the topography. Any value could be chosen for the density, however it is clearly desirable to eliminate the effects of surface features as much as possible by using the average bulk density value.

Here, four methods are used to estimate the bulk density distribution. One of them is laboratory determination of the density of saturated and non-saturated rock samples from surface and drillholes up to 290 m deep. The second method includes the classical approaches of Nettleton (Parasnis, 1972) where the correlation between the Bouguer anomaly and the elevation is minimized. This is based on the hypothesis that the Bouguer anomalies behave as stochastic quantities which are not correlated with point elevations.

The third is a method developed by Parasnis (1972) which is very similar to Nettleton's method. The Bouguer anomaly is considered to be a random error of mean value zero (Figure 2) and a least squares line is fitted to the relation of G_{obs} + 3.086h versus -0.4191h + T. The slope is the required density, h represents the elevation and T the terrain correction.

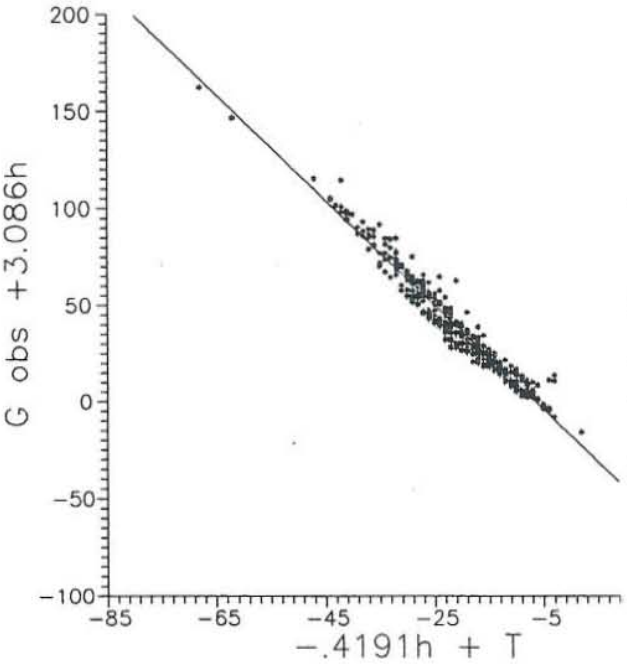

FIGURE 2: Parasnis method for best density choice. Fit line Y = -2.7083X - 17.253

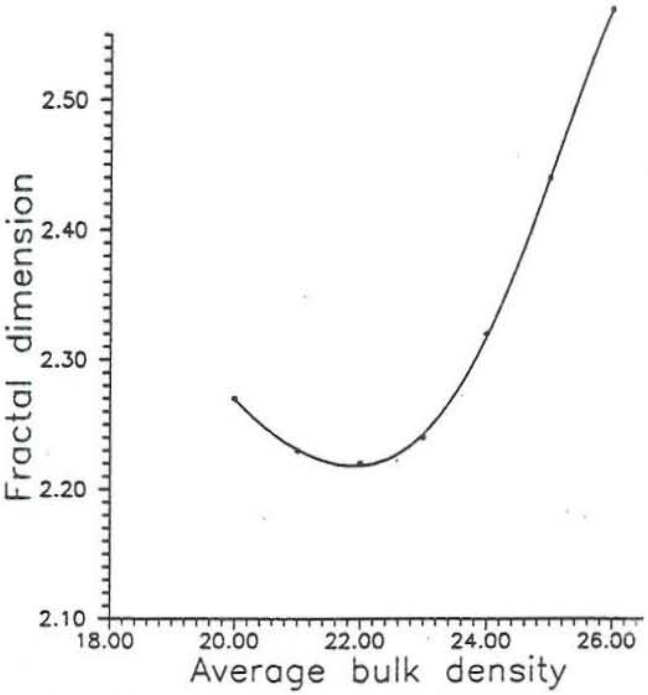

FIGURE 3: Mean density by fractal analysis. The lowest value is the density considered.

Finally, the fourth method applied is based on the fractal properties of the topography (Thorarinsson and Magnusson, 1990). They state: "assuming the gravity field to be of less roughness than the topography, we determine the Bouguer density by minimizing the roughness of the resulting Bouguer anomaly". This roughness is estimated by the fractal dimension of the surface plotting the variance of the Bouguer surface against the distance, which results in a graph on which a linear relationship over a range suggests an estimated self-similarity in the range. For preparing the data, a file was created that includes the greatest amount of data (404 out of 502 gravity stations) within a circular area with an 11 km radii, where the data has the best distribution density of measurements (a mean of 1 per km^2). The density which minimizes the roughness is then chosen (Figure 3).

Table 1 summarizes the results of density determinations. It includes also a density estimate obtained after practising a t test which takes into account the size of the sample, such that when the number of samples goes to infinity, the t distribution and the normal distribution are identical. The fractal analysis turns out to give the lowest density of all the methods. Nettleton and Parasnis give the highest density.

TABLE 1: Density calculations obtained through different methods (kg/m^3)

Method employed	Density
Rock samples	2400 ± 336
t Test	2400 ± 211
Nettleton	2720
Parasnis	2710
Fractal analysis	2230

The range of variation is large, so we start by looking at density values in selected areas, both outside and within the area with the best distribution of measurements. The Nettleton method points out a trend inside the whole area that tends to enhance the density value, for example in the central part, where it gave density values of 2345 kg/m^3 compared to the regional value of 2720 kg/m^3. This can probably be explained by considering the negative anomaly in the centre of the area that consistently appears at different density reductions, and is large enough to influence its surroundings. Several negative anomalies elongated in the direction of the main gradient belts (Figure 4) which may lower the density value are also observed on the Bouguer anomaly map. In subsets to the southwest and north outside the influence of the negative anomaly, a mean density of 2500 kg/m^3 was obtained. The selected density of 2550 kg/m^3 is in between the mean density of the rock samples and the Nettleton density which considers values not less than 2500 kg/m^3 (with the exception mentioned) obtained at the borders of the zone but, nonetheless, less than 2720 kg/m^3.

3.2 Trend analysis

Once the gravity had been reduced to a datum level and the magnetics reduced to the pole, two maps of the respective field anomalies were prepared to give an idea of the regional behaviour of the anomalies according to the data distribution (Figures 4 and 5).

Gridding is a common method but one must be careful in the procedure. In our case, it was performed with the inverse distance interpolation method using a weighting factor of 2, and prepared for use by an FFT algorithm, thus making the grid a multiple of the power of two. When gridding, the information must be carefully treated according to what we are looking for, in order to avoid the introduction of spurious signals that will cause noise (high frequencies) in the subsequent analysis. Furthermore, one must take into account the distribution of the data, in order to avoid shaping the anomaly distributions and giving bias to the possible interpretations in the spatial or frequency domain, due to clustering or edge effects. However, it is clear in the case of magnetics that its inverse dependence to the third power of the distance tends to create a higher frequency signal, which together with the large variation in susceptibility, in terms of up to two orders of magnitude makes the interval between stations inconsistent with the true variation of the magnetic field.

As the stations were not evenly distributed, it was decided to analyze four square areas of ten by ten kilometres with a good coverage of stations, with the exception of the northern part which shows the largest blank area in the southeast corner (Figure 6, Table 2). Originally, a square area of 24 km per side as the largest area with the largest amount of data points was considered as a suitable area to be interpreted, gridded as a square matrix of 32 by 32 grid points. But it was thought to be more advantageous to take smaller areas to avoid possible bias, such as obvious high frequency features not possible to observe in larger areas. More relevant still, each section could be characterized structurally or by density.

For each area, a 16 by 16 grid with sides of equal length was calculated giving 256 grid points which resemble the real station distribution both in gravity and magnetic measurements, with the exception of the northern square. Each zone is characterized by predominant tendencies, or predominant anomalies. Area A0 very likely characterizes the border of a caldera with some intrusions or dense bodies. Area A1 is dominated by a circular anomaly; an attempt was made to model it quantitatively. Area A2 is characterized by a NW trend of extensional structures, part of the Arenal graben. Area A3 has the same predominant trend as Areas A0 and A1, but with frequent intrusive activity related to domes and lava domes.

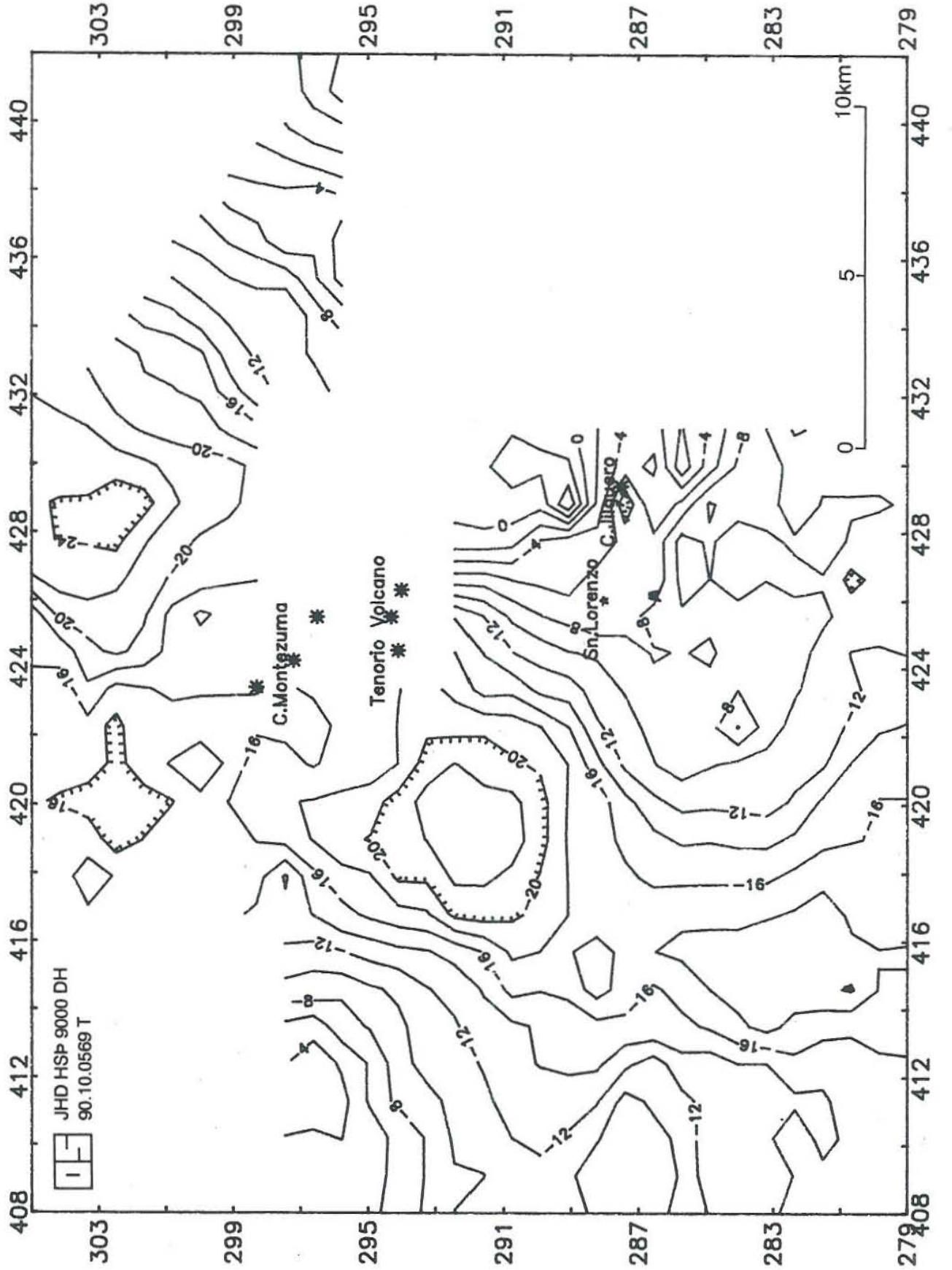

FIGURE 4: Bouguer anomaly map of the Tenorio area, density 2550 kg/m³
Dots show volcanic edifices; tic marks at 2 km interval

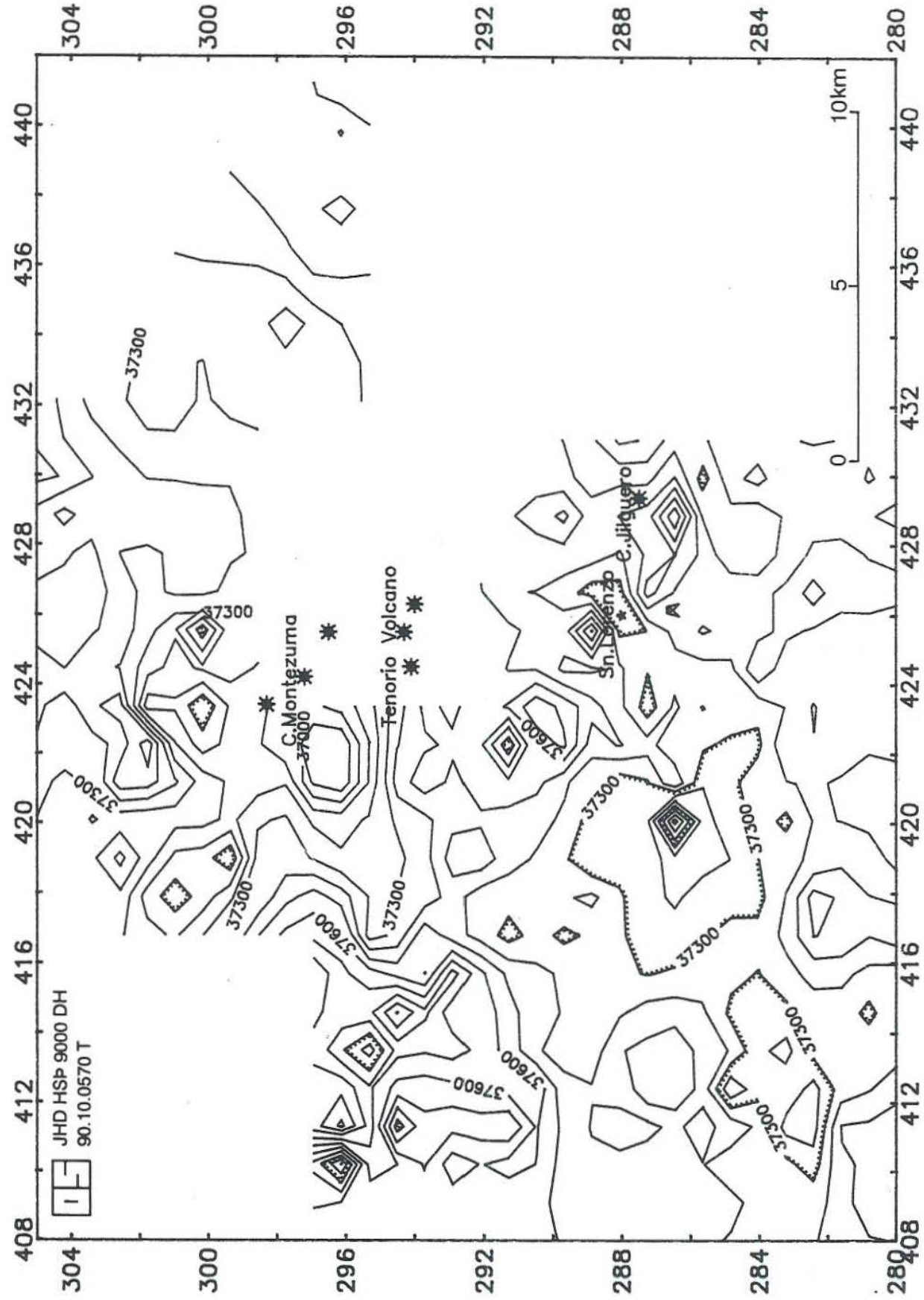

FIGURE 5: Magnetic anomaly map of the Tenorio area. Dots show volcanic edifices; tic marks at 2 km interval

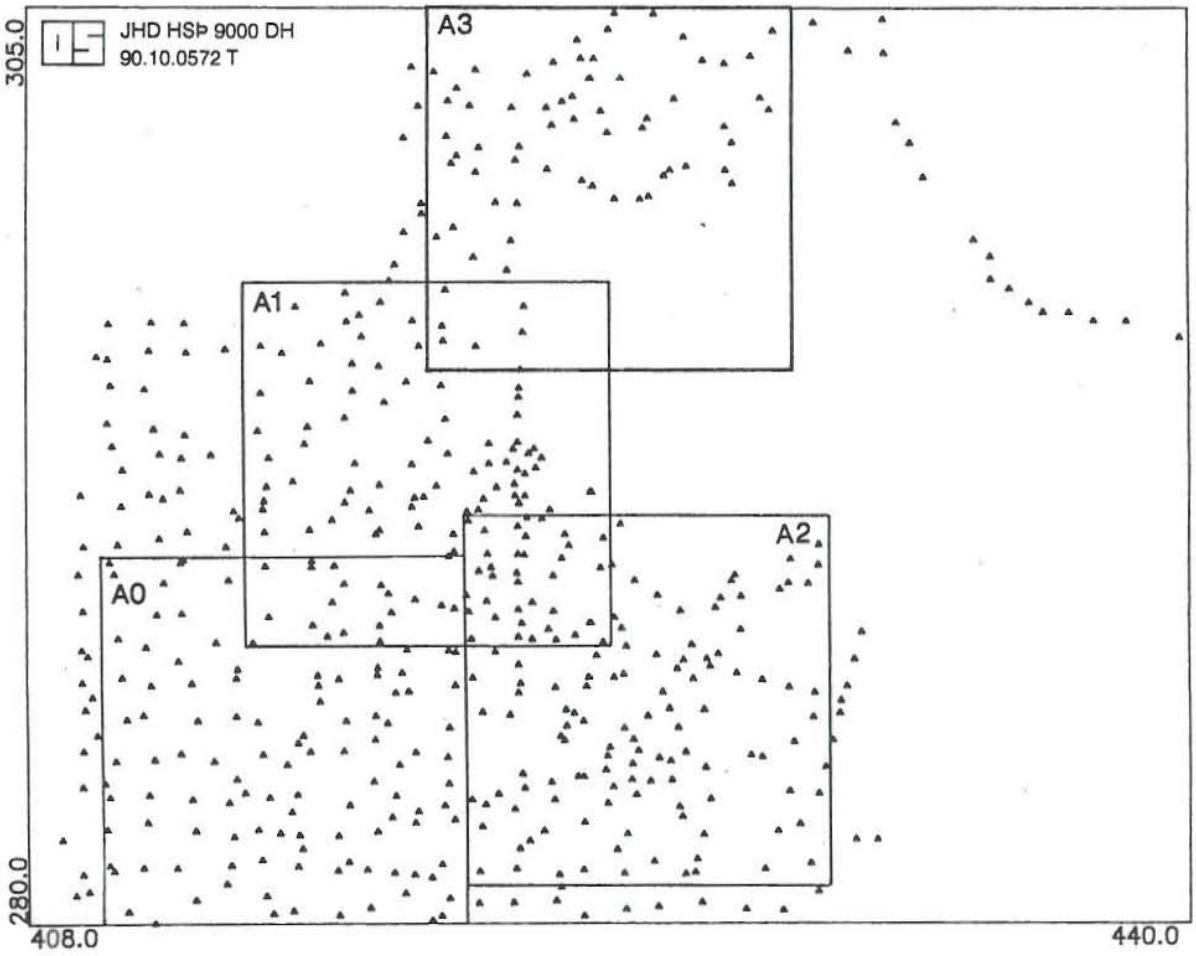

FIGURE 6: Station density distribution; A3 has the lowest density; coordinates are in km

Once the best possible density distribution areas had been selected and gridded, the trend analysis was applied, interpreting the residuals in a statistical sense. The main consideration was to separate the data into two components, the regional geological setting and the local deviations at the working scale. The availability of data becomes very important as these local deviations can be meaningless if we consider features whose sizes are smaller than the separation of stations. In fact, the residual anomalies can be separated by any linear trend, (acting as a high-pass filter) and much more can be done in different trend analyses, resulting in fewer and fewer deviations until there would be no separation of the data. But the purpose of our research must be kept in mind, which is to enhance or isolate the anomalies of interest.

TABLE 2: Statistics of the distribution of the original data

Area	Stations		Coverage
	Grav	Mag	(km²)
A0	128	129	100
A1	134	138	100
A2	145	150	100
A3	63	67	100

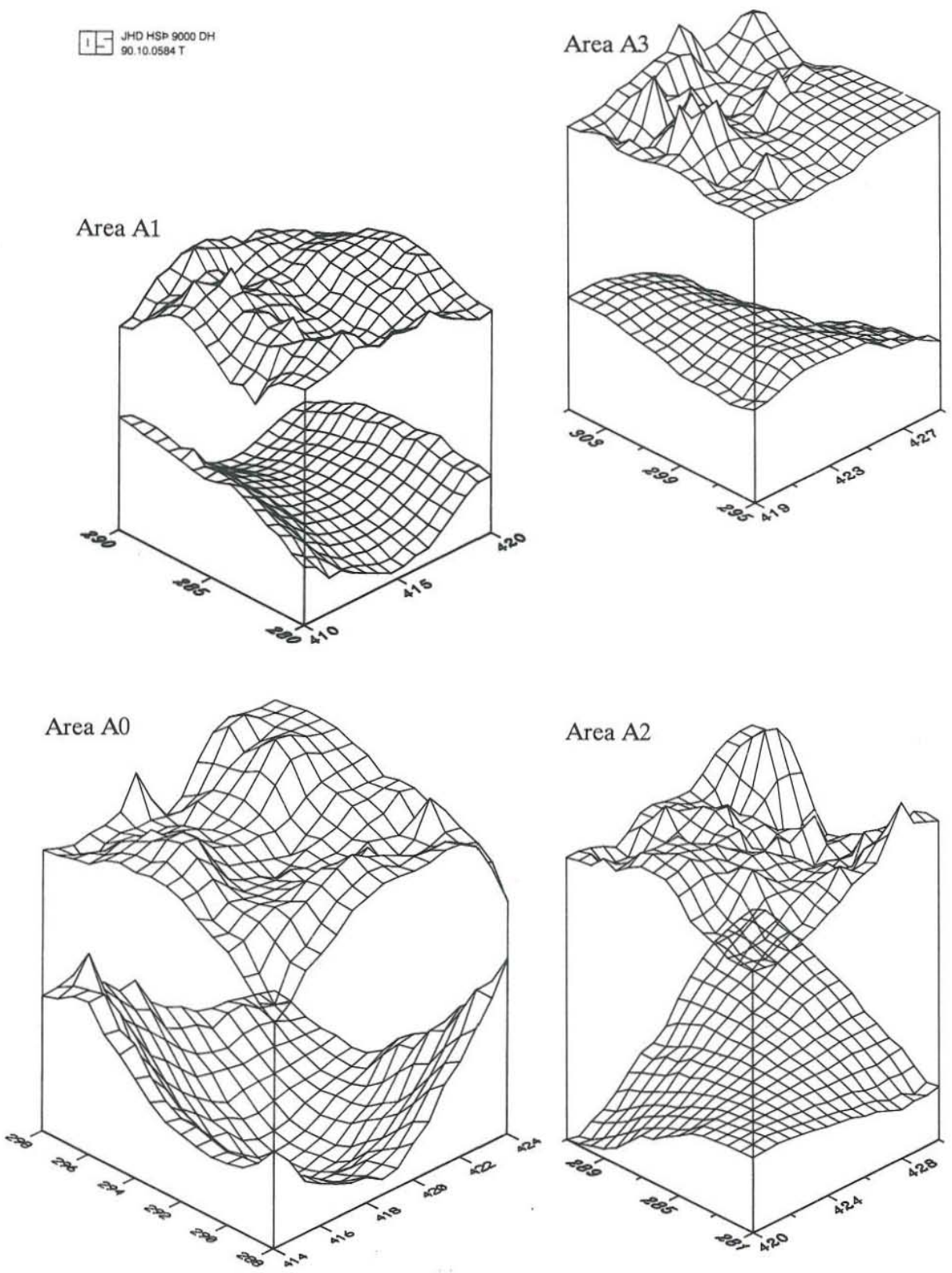

FIGURE 7: 3D outline of residual and regional gravity surfaces obtained by statistical analysis of the trend; upper surfaces show the residuals (coordinates in km)

The trend analysis was carried out analyzing the variance, both the variance about the regression plane and the variance of the regression about the mean, such that the trend can be regarded as a function with less variance about it. In the cases analyzed, the F test gave the probable answer as to whether it was worthwhile or not to continue applying higher polynomial orders to the data.

A linear trend surface would then have an equation like:

$$Y=b_0 + b_1X_1 + b_2X_2$$

where Y represents the gravity value regarded as a linear function of the mean, mutually perpendicular components X_1 and X_2 regarded as coordinates, and a constant value b_0. By solving the system of equations, we will obtain the coefficients for the best linear trend surface fitting in the least squares sense.

For the sake of being systematic, each area was reduced using a second order polynomial in the least squares sense. An ANOVA table (Table 3) was used to decide the best polynomial fit for the regional trend. The results show the second order polynomial to be the best solution for all areas except Area A0, where the ANOVA table suggests a possible fourth order polynomial. If the F test is not significant then we have not gained anything by trying to fit a higher degree polynomial; this is also expressed by the goodness of fit (Table 3) and the percentage of improvement.

TABLE 3: Example of ANOVA table for choosing the best polynomial order

```
==========================================================================
Analyzing data file: a01.xyb

Polynomial of order          2


ANOVA - Analysis of variance table.

Source of        Sums of     Degrees of          Mean        F test
Variation        Squares        Freedom        Square

Regression       1535.58            6          255.93        98.78
Deviation         331.65          128            2.59        98.78
Total Var.       1867.23          133

Goodness of fit:  82.2%
```

Figure 7 shows a 3-D outline of the residual anomalies (upper surface) after the regional trend (bottom surface) has been subtracted. Note how Areas A0 and A1 show more complex planes; in particular, Area A1 has a circular negative anomaly of about 4 km in diameter.

3.3 Frequency analysis

The frequency analysis can be seen as an extension of a polynomial trend surface analysis with three space coordinates, in our case, latitude, longitude and the Bouguer value transformed in terms of frequency, direction and amplitude. The frequency analysis was done by means of fitting a series of harmonics of sine and cosine waves to the data. If there are some features

with linear (space domain) or periodic (frequency domain) trends, this type of analysis becomes useful.

The programme STRIKE (Thorarinsson and Magnusson, 1989; Thorarinsson et al., 1988) makes use of the two dimensional Fourier transforms as a series of one dimensional discrete Fourier transforms, first transforming rows and then columns, of which the end result is the amplitude spectrum, outlined as spatial frequencies increasing radially outwards from the centre, coinciding with the regional values with low frequencies located at the centre (Figure 8). This double Fourier analysis is combined with two dimensional filtering to produce filtered space domain maps. The filters available were used to isolate anomalies, by removing or enhancing linear features, or by removing or enhancing spatial frequency ranges.

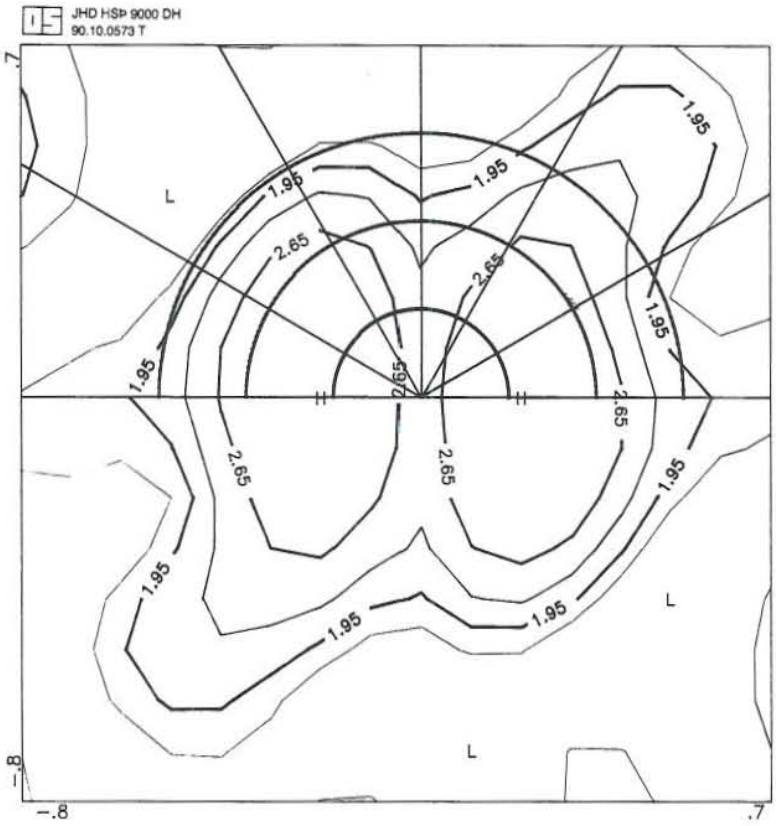

FIGURE 8: Amplitude spectrum of Area A2, showing a major linear trend at 130°; the angle starts at zero at the left side and increases clockwise; the central value is the DC bias and the Nyquist frequency is reached at the edges.

STRIKE also offers other frequency operators by means of linear transformations of gravity and magnetics, using convolution factors that operate as multiplication factors in the frequency domain. These other frequency operators are: analytic continuation, vertical and horizontal derivatives and the transformation of the magnetic field to a pseudogravity field using the frequency data (keeping in mind that the highest frequency to be determined is constrained by the station separation. In our case the Nyquist frequency has a wavelength of 2 km).

Some problems like leakage are inevitable where nonperiodic waveforms are transformed. In our case, these were treated separately as edge effects and regional trends and worked out in the space domain. This is carried out by windowing the data as the leakage depends upon

the window shape and how the waveform fits into the window. This simply means lowering the signal to zero at the edges of the gridded area. The window mostly applied was the Hanning window.

Next, the power spectrum, which is the estimation of the contribution of different harmonics to the variance, is calculated (but like all estimations may deviate markedly from the true population spectrum), and then used for further filtering, suggesting (Figure 8) anomalous narrow features, in this case from 120° to 150°, suitable for isolation by means of directional filtering.

All of this frequency analysis was made by means of the FFT algorithm which realizes a special matrix operation that, according to Davis (1986), may be compared "to constructing a circular matrix in which the origin of series is placed at the centre and the data sequence is "wound" around the centre, proceeding then by shifting multiplications and additions between adjacent entries".

Once the Fourier coefficients have been calculated, the two dimensional raw spectrum can be calculated by an extension of

$$S^2 k_1 k_2 = (\alpha^2 k_1 k_2 + \beta^2 k_1 k_2 + \tau^2 k_1 k_2 + \delta^2 k_1 k_2)/4,$$

where S^2 is the variance of the kth harmonics in each dimension, and Ak_1k_2 the amplitude of the waveforms that are expressed by the square root of the sum of the coefficients.

The power is an expression of the variance and measures the variance contributed by k_1th and k_2th harmonics to the total variance of Y. In a simple way any curve that has a sinusoidal form can be written as

$$Y_k = A_k \cos(k\theta - \phi_k),$$

of which direct expansion is the distribution of Y_{ij} as a double Fourier series.

Each area is first analyzed in terms of regional features and then higher frequency anomalies are analyzed. The analytical procedure is always guided by the geological knowledge we have of the area, the general features of the unfiltered gravity or magnetic maps and the power spectra of these maps.

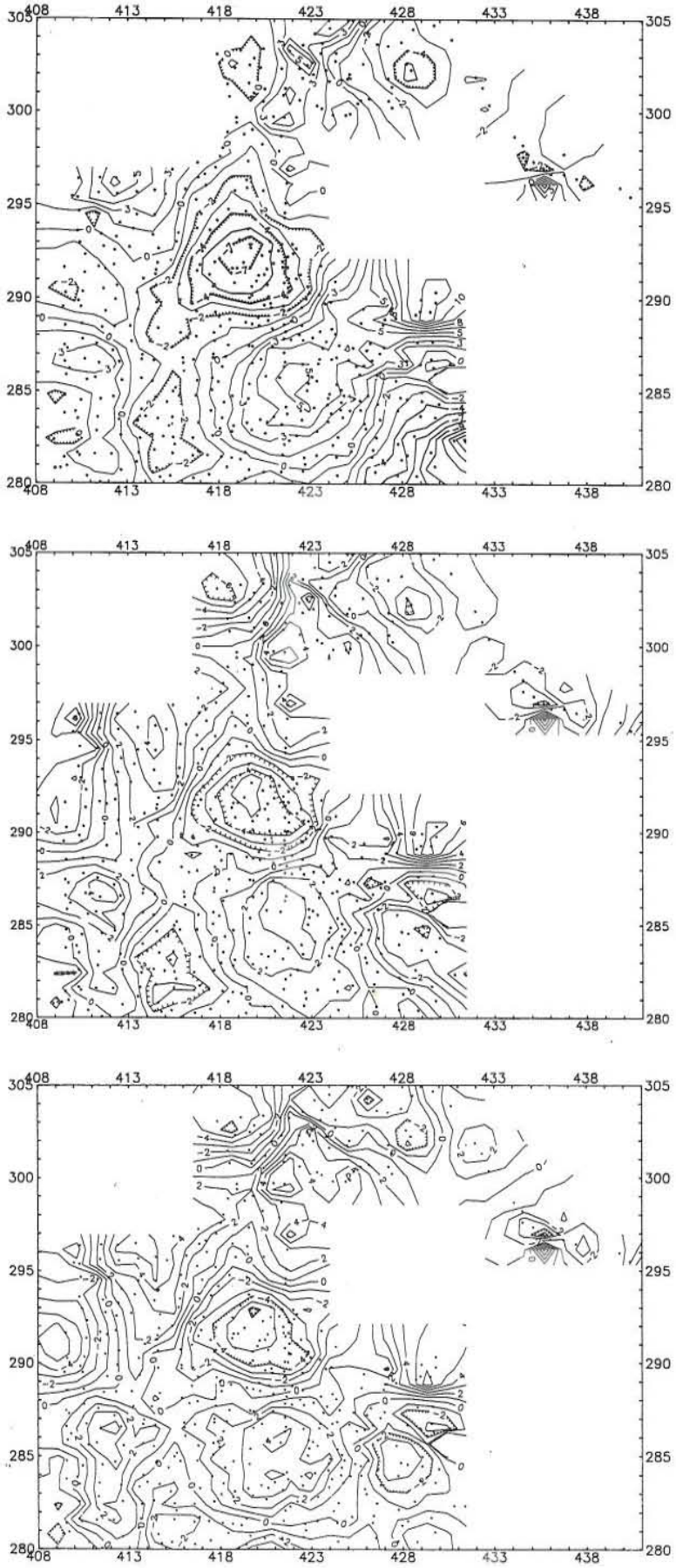

FIGURE 9: Bouguer gravity after the substraction of different least squares polynomials; 2nd order polynomial at the top, 3rd in the middle and 4th order at the bottom. Observe how, in the lowest figure, the negative anomaly to the south and the Arenal graben are substituted by a circular negative; both become less clearly defined.

4. INTERPRETATION

The interpretation stage started by a simple observation of the whole map, later subdivided for the sake of doing a detailed analysis. It was possible to infer some of the broad structures that influence the regional behaviour of the anomalies. Figure 9 shows the Bouguer anomaly map after the removal of 2nd, 3rd and 4th order polynomial trends respectively, with the station distribution included.

In the map showing the subtraction of a second order polynomial, a pair of gravimetrical "ridges" 5 km long are seen in the southwest and to the north of the area (coordinates 300/423) with an almost N-S strike. A broad circular high to the southeast is clearly observed; this is shaped by two gradient belts that run NE-SW, narrowing at around 286/424, isolating, as a result, this wider anomaly from the increasing gradient towards the Jilguero mountain. Ample negative anomalies follow the same trend as the previous belts, and possibly continue to the north. In the residual from the third order polynomial (Figure 9), the ridges are well observed with a suggested NNE-SSW linear continuity, interrupted only towards latitude 300. The relatively positive anomaly near Sn. Lorenzo river is now more circular and tends to become thinner towards the northeast near the thermal alteration zone indicated on the geological map. The gradient belts are not well defined, but a NW-SE negative lineament appears which could be related to an extension of the Arenal graben (Figure 1).

In both residuals, three large negative anomalies in both extremes of the area (north and southeast) and in the centre are clearly seen. But after the substraction of a fourth order polynomial surface, the negative anomaly to the south disappears (Figure 9). The appraisal of the fourth order residual shows the ridge-like anomalies as local anomalies losing their elongated character that have been almost totally removed and the possible Arenal graben becomes an association of two small negatives; the central anomaly persistently appears, confirming its influence.

On the magnetic map (Figure 5) it is possible to observe an extended negative all along the southern part running WSW-ENE which, according to its size, can exert a great influence on the local anomalies. This anomaly will be traced in A0 and in A2.

4.1 Results

The preliminary results given here must be submitted to later analysis by the multidisciplinary group that has been working in the area, as it is clear that the inverse problem is difficult to assess from a single point of view, in our case only gravity or magnetics.

We draw the attention of the reader to the fact that each of the areas is characterized by a particular anomaly and that each of these areas covers 100 km^2. For comparison purposes, maps with the original data are supplied (Figure 10). The processing maps include some structures and alteration zones shown in the geological map (Figure 1) for the geological orientation of the reader. All coordinates refer to the location of the bottom left corner.

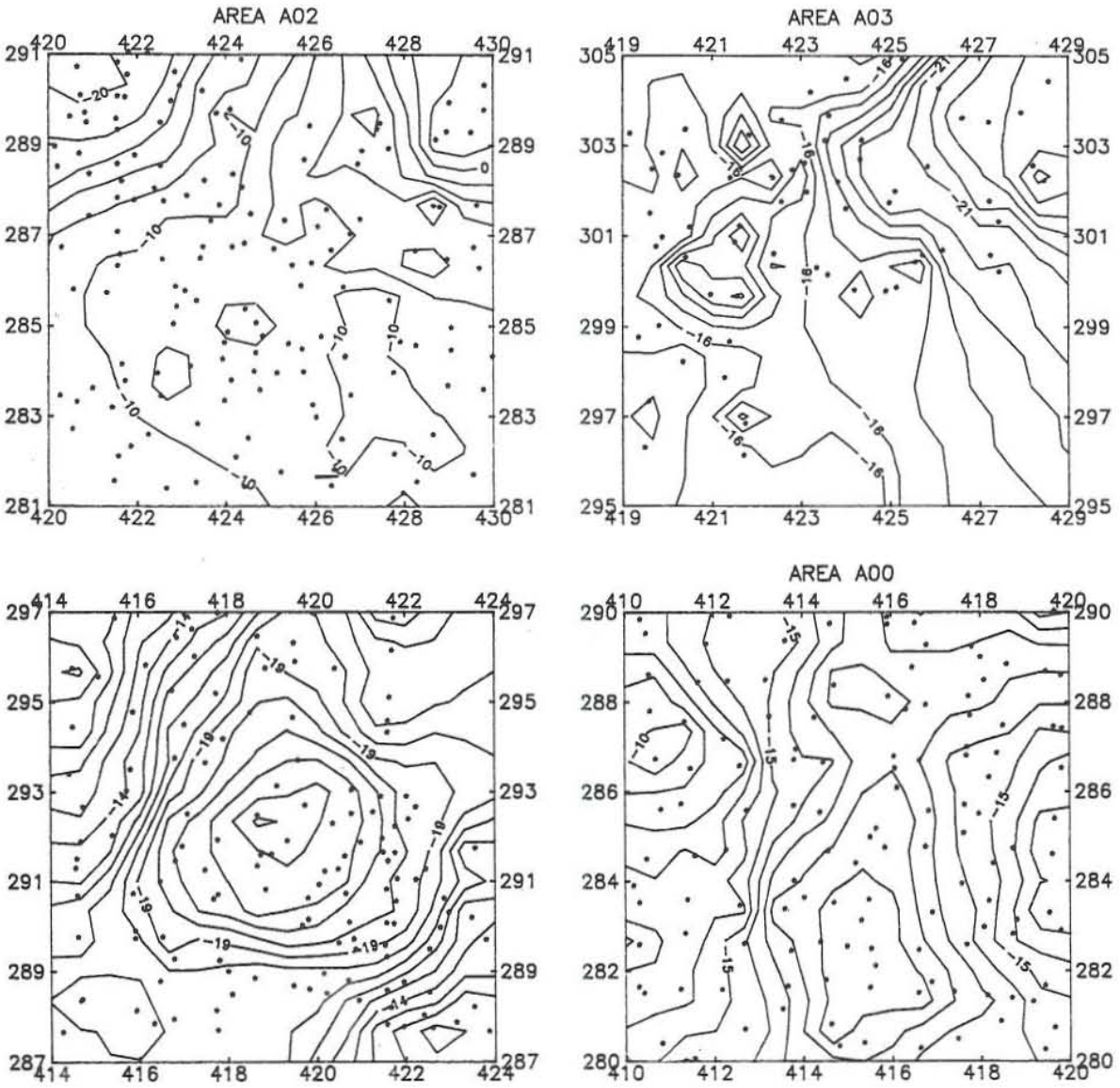

FIGURE 10: Original data with the measurement stations; tics marks at 2 km interval

4.1.1 Area A0, coordinates 280/410

This area is characterized by a negative anomaly in the middle (Figure 10). Geologically it coincides with avalanche deposits, and pyroclastic flows from the latest stage of volcanic activity. The topography is smooth and flat.

The gravity amplitude spectrum map (Figure 11a) suggests one broad north-northeasterly trend occupying more than 50% of a quadrant. Only at the edges in the high frequencies is it possible to infer a very smooth lineament between 90° and 120°, but it is not very well defined. Nonetheless, these directions are repeated on the magnetic spectrum map (Figure 11b), clearly enough to be isolated.

The trends at 35°, 75° and 155° on the magnetic spectrum map are related to the previous ones

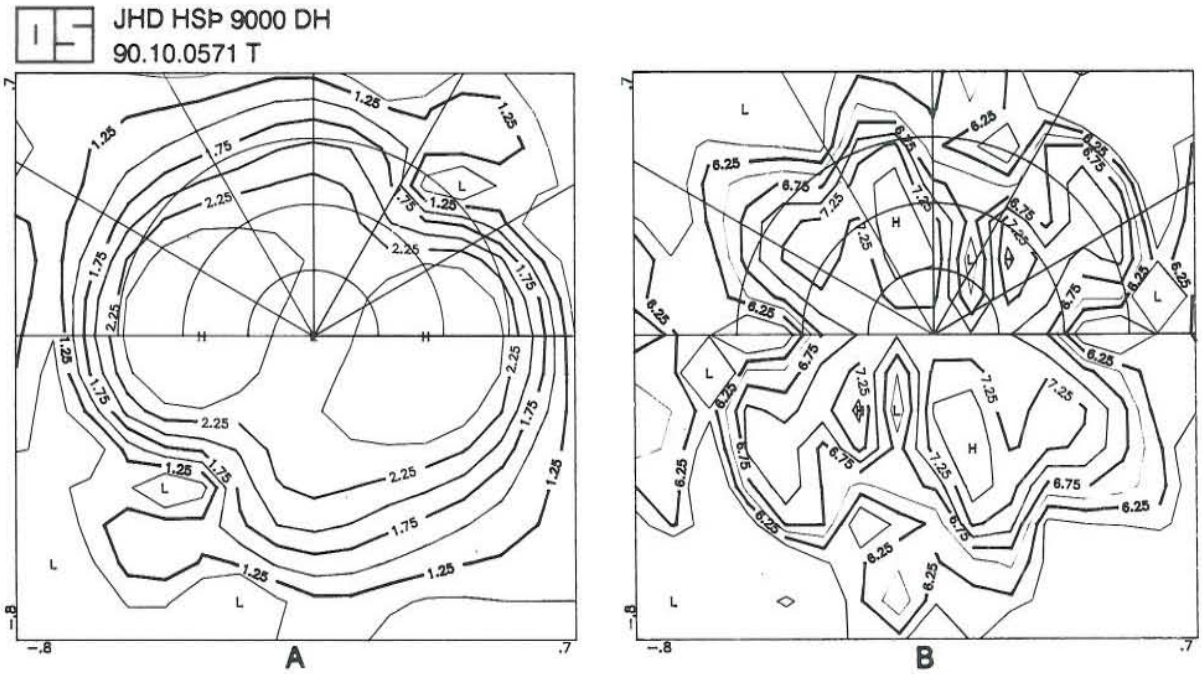

FIGURE 11: Gravity (A) and magnetic (B) amplitude spectra of Area A0; observe broad features at 35° and 150° in both maps

in the gravity. As a consequence, the magnetic data were considered to be more suitable for analysis, and are the ones shown.

Directional filtering on the magnetic data at 155° reveals sharp NW-SE gradients that follow the pattern of the Arenal graben (Figure 12b). This trend seems to prevail as the oldest fault

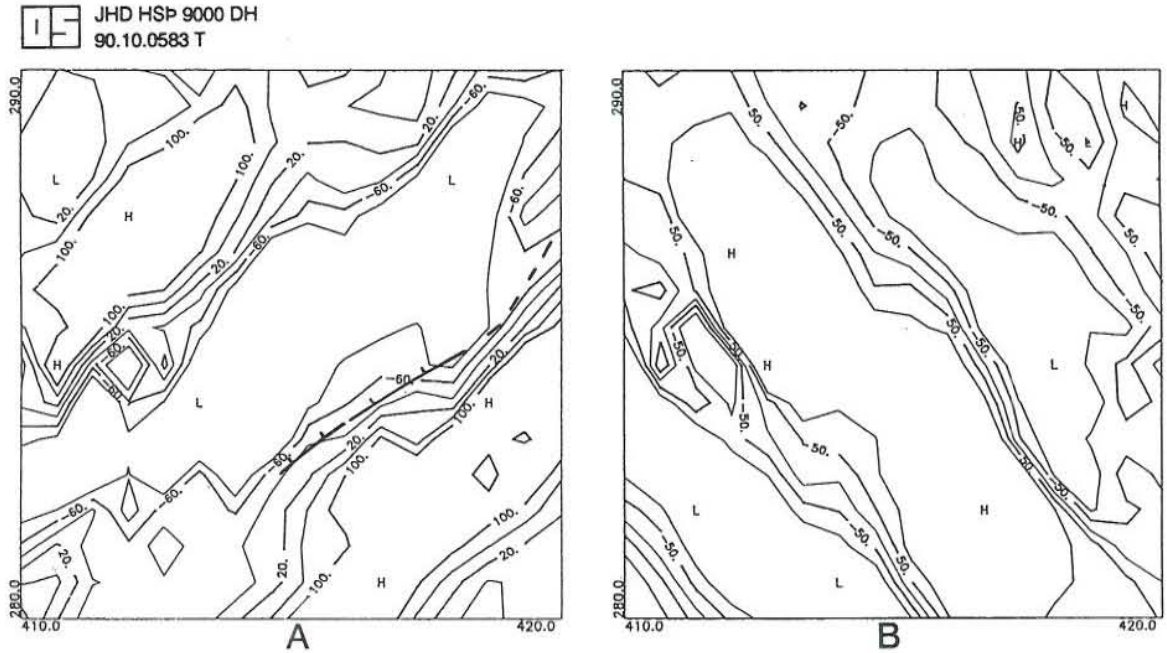

FIGURE 12: Directional filtering of the magnetic map of Area A0, reduced to the pole; magnetic spectra at 35° and 150°, A and B respectively; in both cases, a Butterworth fanpass filter is used. Structures from the geological map are indicated. The area is 100 km².

system. The features around 30° were also studied by directional filtering. They could be related to the NE-SW faulting that is considered much younger than the regional faulting that originates the Arenal graben (Figure 12a).

At first glance, the low frequencies (Figure 13) resemble the original data (Figures 10) but enhance three highs; in our case, a low-pass filtering of the gravity data (Figure 13b) gives two highs that suggest 1) a ridge-like form narrowing to the centre, located in the southwest with a NNE-SSW trend, and 2) a large positive to the west that later will be shown to be related to thermal alteration.

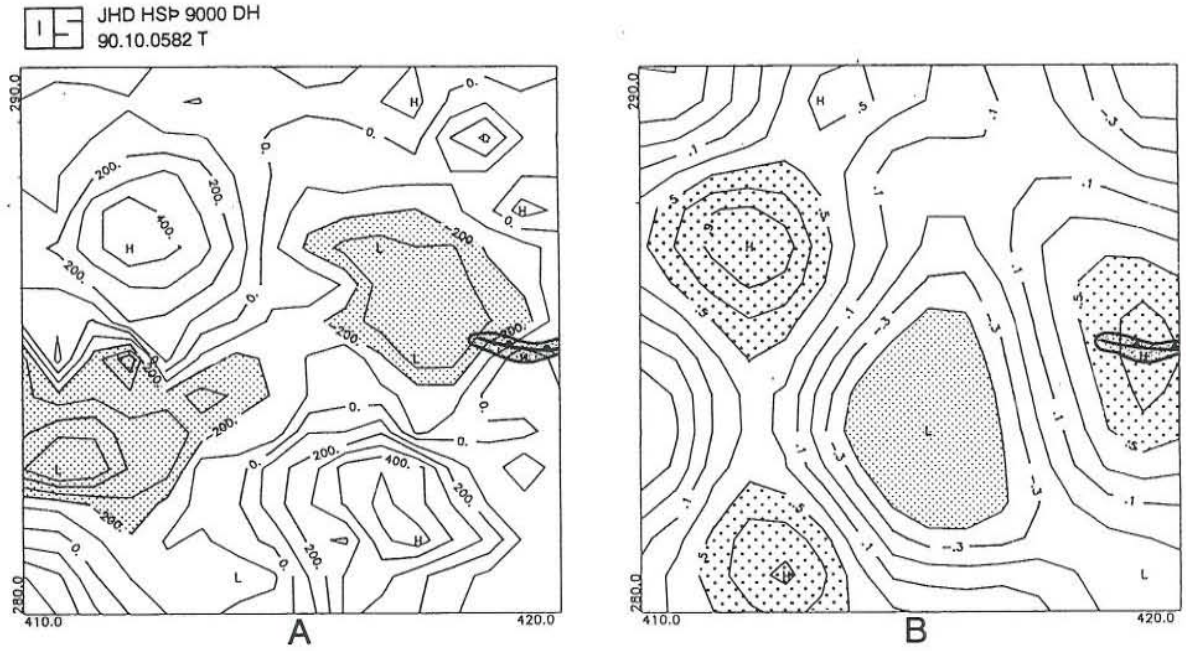

FIGURE 13: Magnetic map reduced to the pole (A) and gravity low-pass filtered map (B) of Area A0 (cutoff frequency at 2). Observe a magnetic negative belt from southwest to northeast and the superficial alteration coinciding with a gravity high. Coordinates in km

Searching in the magnetic map (reduced to the pole), an ENE-WSW negative belt is clearly revealed which extends all along the area, and which can be traced further in Area A2. Furthermore, this tendency is well observed in the magnetic spectrum at 75° (Figure 13a). Regarding the sharp gradients in the directional filtering as suggested faults, the gravity highs will probably be the result of the mixed activity of two fault systems.

Correlating the low-pass filtering with the reduction to the pole, it is worth noting that some of the large negative magnetic anomalies can be associated with positive gravity ones. This is especially noticeable in the caldera rim at the right side of the area, where the convergence of several factors indicate a relatively large positive anomaly with an altered zone superficially expressed; and two morphological features that are identified in the geological map as traces of antique rims. To the west, the coincidence with gravity highs is not well correlated; instead, they coincide with materials of different susceptibility as by-products of hot water rising or that rose through the intersection of structures.

According to the magnetic amplitude spectrum two systems of faults are suggested, one WNW-

ESE and the other NNE-SSW, the latter being rather smaller than the other. The second is observed in the high frequencies, which could imply shallow faulting or neo-tectonic activity. The pseudogravity map (Figure 13a) shows the predominant influence of the magnetic belt along this area.

4.1.2 Area A1, coordinates 287.5/414

Almost all the area is covered by a large negative gravity anomaly that strongly determines the behaviour of the regional trend. The regional trend turns out to resemble a paraboloid that compensates for what here is considered a crater structure (Figure 7). This central anomaly is associated with the filling of an eventual depression or crater by huge pyroclastic deposits.

Such being the case, the gravity amplitude spectrum does not show clearly the main trends, as this circular anomaly overcomes all the signals. After low-pass filtering, the gravity map (Figure 14a) reveals two positive anomalies that may be considered an extension or continuation of the caldera border to the southeast and a large low in the middle, slightly elongated to the southwest. This symmetrical shape and distribution may contribute to the enhancement, producing a large almost circular negative, as can be seen in the original data (Figure 10).

This large deficiency in mass correlates to a positive anomaly on the magnetic map. To make the comparison to the gravity data easier, we have transformed the magnetic data into pseudo-gravity data, after first reducing it to the pole (Figure 14b). A central magnetic high correlates to the regional gravity low. A pair of negative anomalies in the pseudo-gravity map coincides with the gravity highs observed at the caldera rim, and in fact, delineate it more clearly.

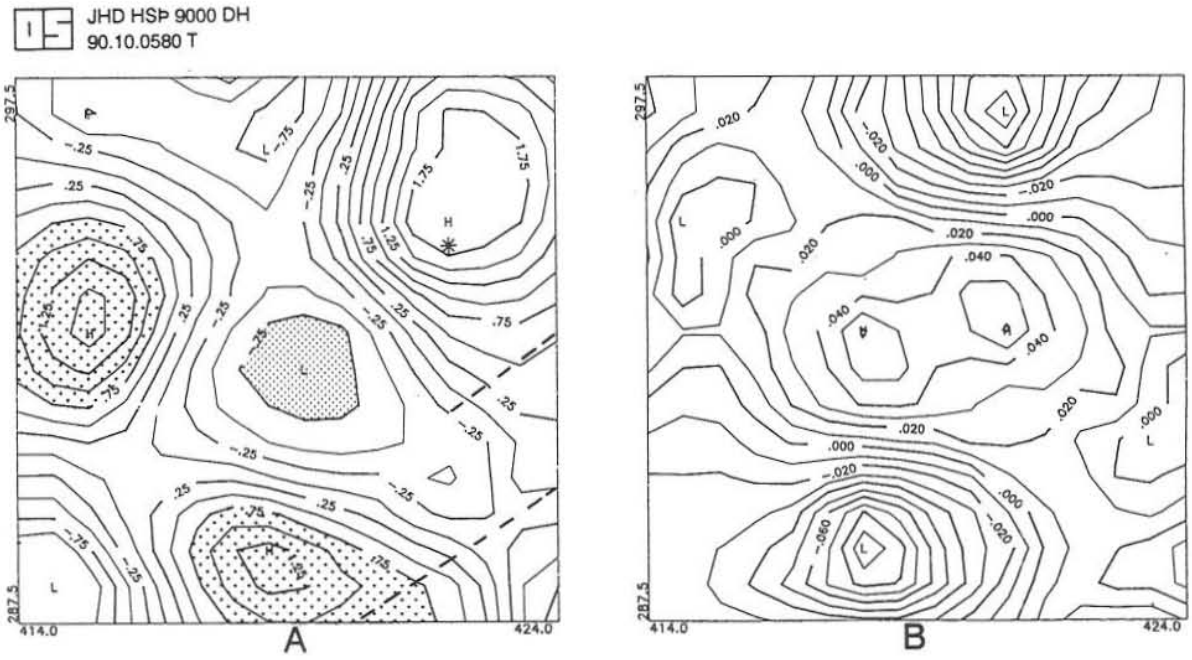

FIGURE 14: Gravity (A) and pseudogravity map (B) of Area A1. The gravity map is low-pass filtered; it shows two shaded highs at the bottom and to the left on the map which are interpreted as showing the caldera rim. The pseudo-gravity map is calculated from the magnetic map, after reduction to the pole. Magnetic lows are associated with the caldera rim, and a magnetic high in the centre of the map compares to the regional gravity bowl (see Figure 10). Coordinates in km

A dipolar nature of the positive pseudogravity anomaly at the centre in both highs coincides with deeper points in the gravity outline and correlates with the nature of the subsequent infill. Later in this report the deficiency in mass will be estimated, considering as its cause two mass anomalies that, together, produce the larger anomaly observed in the gravity map of the whole area.

The correlation of gravity to magnetics is well establish in this area and in both maps offered Figure 14) it was possible to postulate an extension of the caldera rim.

4.1.3 Area A2, coordinates 281/420

This area is characterized as a lava plateau at the base of two volcanic edifices, the Jilguero mountain and another unnamed. It coincides with an extended relative high with smooth anomalies (small range of variations).

Figure 8 shows the gravity amplitude spectrum of this area. A narrow feature is observable clearly enough to be isolated and, in fact, was filtered with directional filtering at 130° with a band angle of 60°. The result is shown in Figure 15b, showing three gradient zones associated with the predominant fault system, indicated as thicker solid lines in the figure. In the original data (Figure 10) it is not possible to distinguish the influence of the Arenal graben, which has a NW-SE linear trend. In Figure 15b, it can be seen that the graben may be extended throughout the area from the southeast to the northwest. In fact, these faults correspond with the older and more notable system. In general, three fault generations can be seen; 1) faults associated with the graben, 2) faults that could represent a slight rotation of the first and 3)

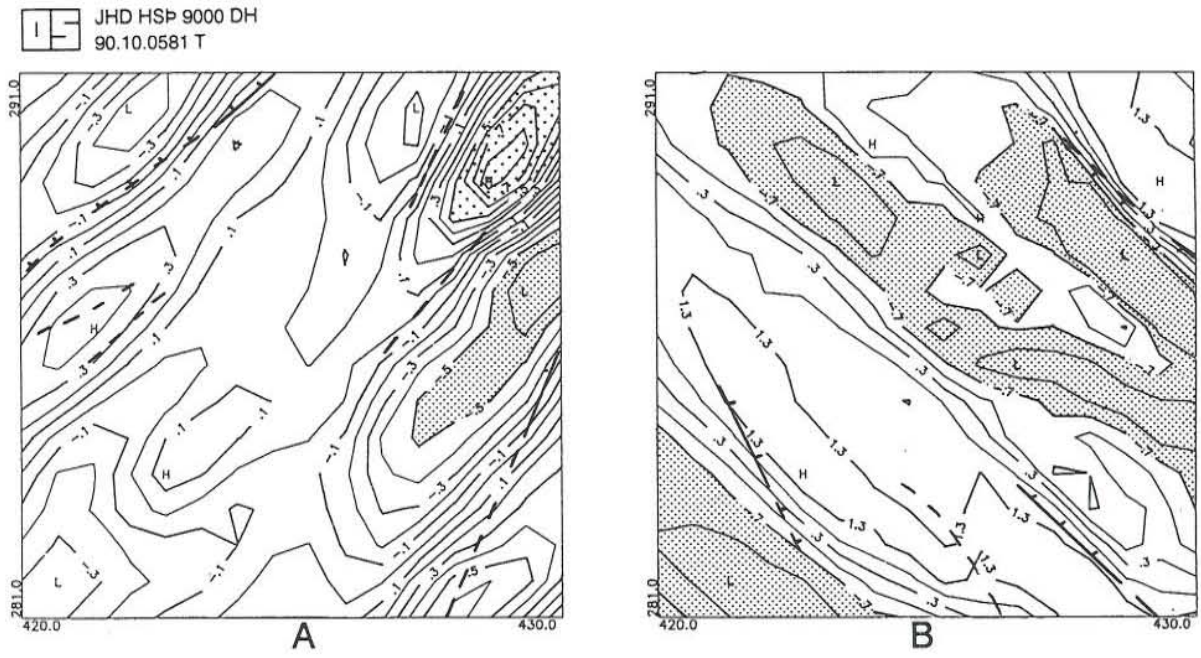

FIGURE 15: Directionally filtered gravity maps of Area A2. A was filtered with a Butterworth bandpass at 40°. Observe a small horst and graben in the upper right corner. A Butterworth fanpass was used at 130° in B; note how the Arenal graben can be extended from southeast to northwest according to the indicated structures shown on the geological map. Coordinates in km

a last one that cuts the others, depicted in the graben as small isolated blocks confined by faults. From the gravity interpretation it is not possible to extend the faults to the southwest, though a sharp gradient suggests a structure with a downthrow to the southwest, a trend that is followed in Area A0 with a similar direction.

By exploring the gravity amplitude spectrum in the high frequencies at 40° with a fanpass filter or by means of a bandpass filter in the same section, it is possible to follow a less important fault that cuts the previous one. The gradients show sharp edges again where these systems appear. They are apparently less elongated, forming small grabens, intersecting the other and associated horsts noticeable in the northeast corner. This trend is observable in Figure 15a and in Figure 16, coinciding with smaller negative anomalies.

A strong ENE-WSW tendency appears in the magnetic map reduced to the pole (Figure 16a), that was correlated with the low-pass gravity map. In Figure 13a, a continuity is shown from A0 up to almost the northeast corner. A magnetic negative belt is correlated with a positive gravity anomaly of almost the same direction, observed in the gravity low-pass filtered map (Figure 16b). In a very rough way, this belt resembles the caldera rim indicated in the geological map (Figure 1). This may be interpreted in terms of fossil activity related to the caldera formation. Again, it is worth noting that the relative coincidence of highs on the gravity map can be superimposed onto the negative magnetic anomalies. This is especially visible in the anomalies to the west where the intersection of two rims was mapped on the geological map. It is also possible to infer the predominance of relatively nonmagnetic material to the northeast. It is very likely that this belt does not form a continuum, but represents an average behaviour of the magnetic field. Major faulting has been recognized by means of frequency

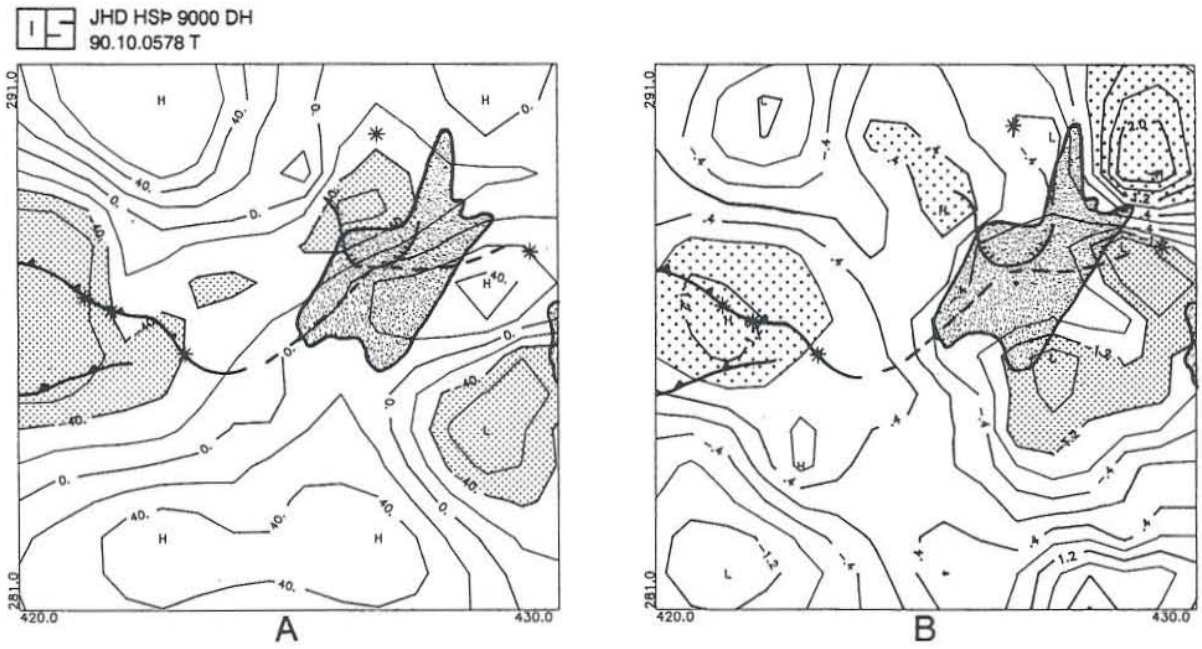

FIGURE 16: Low-pass filtered maps of Area A2. A is the magnetic map reduced to the pole after filtering with a Butterworth low-pass filter, showing a negative belt continuing from Area A0 (cutoff frequency at 2). B is the gravity map filtered with a Butterworth bandpass showing a trend of gravity highs that roughly resemble a caldera rim; and a relative low coinciding with a postulated small graben (cutoff frequency 3). Coordinates in km

analysis, the extension of the graben is suggested, and the occurrence of a small graben and horst are proposed.

The coincidence of two factors occurs in this area: one is the fracture intensity (the highest recognized), and the other is the highest thermal gradient recorded. Moreover, the resistivity basement becomes shallower towards drilled gradient well no. 4 (Figure 1), and this happens within a sunken area. The pseudogravity map mainly shows the predominant influence of this negative belt (Figure 16a).

4.1.4 Area A3, coordinates 295/419

This zone can be characterized by the occurrence of domes and lava domes in great volumes and on areal extension towards the northern side (Bijagua lavas on the geological map) dating one of the final stages of the volcanic activity.

Unfortunately, this area lacks a good density of stations due to the topography and the current exploration stage. This lack of data makes a detailed study difficult, because it exerts a particular influence on the amplitude spectrum introducing noncorrelated features, in our case very broad ones that cannot be clearly isolated.

Working at low frequencies on the magnetic map we found a narrow ridge confining a central area of lows (Figure 17b); this almost coincides with relative highs well defined in the highpass gravity map (Figure 17a) extending from the NNE-SSW and especially observable at the centre of the area. There are also three small highs of short wavelength extending almost NE-SW on the gravity map (Figure 17a), that can be correlated with three lows on the magnetic map; one of these points is within a sunken structure. The pseudogravity map (Figure 17b) resembles the gravity map, showing a good correlation between the two methods.

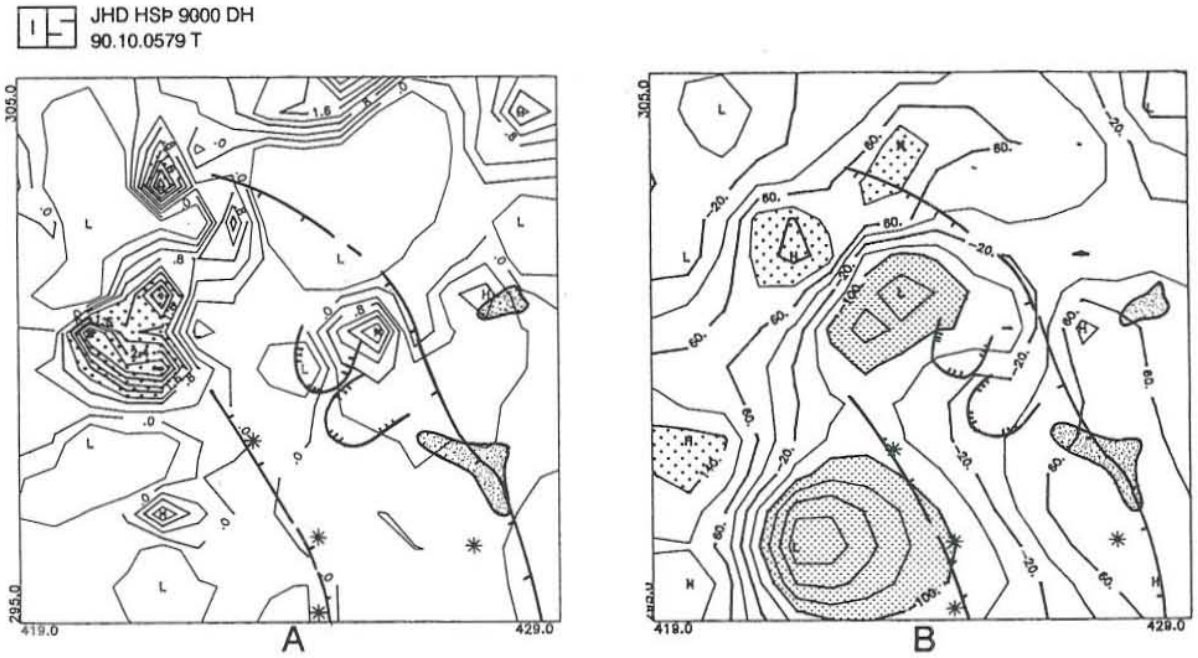

FIGURE 17: Gravity high-pass (A) and magnetic low-pass (B) maps of Area A3. Observe in A what is postulated here as intrusives arranged in an almost N-S direction and small highs from southwest to northeast. In B, a ridge-like form follows the previous one with broad negatives in the centre. Coordinates in km

At 125° in the high frequencies, a good correlation with the evident NW-SE faulting in the zone was found. Coming from Fila Chiquero (see geological map) a NW-SE fault has the strongest signal. The frequency analysis made it possible to suggest other, almost parallel, faults. Each fault can be traced in three gradients belts observed in Figure 18. Although an attempt was made to trace the Fila Chiquero fault across the entire area, the fault is only partially defined due to the absence of data.

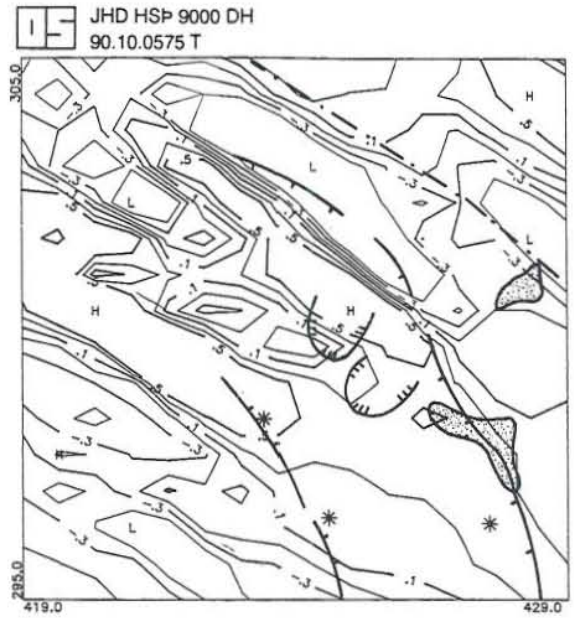

FIGURE 18: Directionally filtered gravity map of Area A3; filtered with a Butterworth fanpass at 125° with a cutoff angle of 5; coordinates in km

4.2 Mass estimation

As the central anomaly seems to be relatively larger than the other ones, it was a good candidate for mass deficiency estimation. In the residual, it is possible to observe how this anomaly decomposes into two, enlarged to the southeast, and how the anomaly has a sort of dipolar shape with two lows in each extreme, showing the assymmetrical shape of the anomaly. It is very likely that the anomaly is a mixture of some faulting, with a simple deficiency in mass due to crater activity.

The estimation of mass was done from the residual gravity map by means of the Gauss theorem which, due to symmetrical considerations, can be reduced to:

$$M = 1 / 2\pi G \, f_s \, A_s \, ds$$

In LaFehr (1965) three sources of error for this type of determination are pointed out; 1) limited coverage, 2) effect of curvature, 3) the effect of numerical integration. The method is highly sensitive to the first one and to depth; LaFehr offers curves for mass correction according to different modelling of depth, width and thickness.

In Table 4, a summary of the results is presented including the mass correction after simple

modelling with a prism of 500 m at 0 depth. As this anomaly is clearly a 3D anomaly, no attempt was made for an accurate 2D model. The total mass deficiency is no less than 4.42×10^{12} g but, as was said previously, the effect may be enhanced due to faulting. In theory, all the masses in column 6 must be the same.

TABLE 4: Mass estimation

milligals	km² *mgal	$Mass_0$	$\delta g_z/(\delta g_{zmax})$	%M	M
-1.75	-0.98	0.234	1		
-1.5	-2.278	-0.54	0.86	0.5	-1.04
-1.25	-2.675	-0.639	0.71	0.65	-0.98
-1	-3.725	-0.89	0.57	0.73	-1.21
-0.75	-3.810	-0.910	0.43	0.76	-1.19

$Mass_0$ = Mass without correction,
$\delta g_z/\delta g_{zmax}$ = Ratio of amplitudes of the vertical component,
%M = Percentage of mass corrected, obtained from correction curves,
M = Total mass, corrected.

5. CONCLUSIONS

Based on the signal analysis, a structural conclusion is suggested in Figure 19. It confirms a strong northwest-southeast tendency in probable association with the Arenal graben formation; this tendency is postulated to extend all over the southern part of the Tenorio area. A second system was postulated almost perpendicular to the first one, whose interaction is solved in the case of Area A2 as a small graben within the Arenal graben, together with an associated horst (both shaded in Figure 15a). It is very likely that both systems are well developed to the southwest, confirming an elongated almost N-S anomaly (see Figure 13a), with its western side deeper than the eastern. A caldera rim is proposed towards the centre. Its resultant anomaly strongly influences the others, giving a sort of continual gradient belt.

In the north (Area A3) the faulting seems to follow the circular fault that extends from Fila Chiquero. These are more recent and probably related to the collapse of a larger structure (ICE, 1989). The interaction of these faults results in the partial isolation of basement blocks and/or intrusives that become shallower. It is recommended to densify the measurements in Area A3, to improve the interpretation of the spectral analysis.

From the postulated structures it becomes evident that the largest density is in the southwest in Area A2. Based on a possible fracture permeability, the large superficial alteration, and the highest thermal gradient registered near the sunken area, Area A2 can be considered to be of geothermal interest for further studies. The frequency filtering, especially on the magnetic map reduced to the pole, reveals the occurrence of large negative anomalies extending all over the southern part in a quasilinear fashion, especially in Area A2, roughly resembling the caldera border to the northeast and with a correlating large negative and gravity high to the west, both extending into Area A0. If these magnetic lows occur due to thermal metamorphism such that the magnetic properties are lost then it is possible, either now or in the past, for a shallow heat source combined with faulting to effortlessly cause the rising of fluids, altering large areas. It can be argued that a partial confirmation of this is shown in the coincidence of the negative anomaly inside the sunken area in Area A2 that has a widespread superficial alteration even of the younger tephra (ICE, 1989). The fracturing could easily be much more intense, on account of high fracture permeability favouring the alteration in smaller domains of faults or blocks that facilitates the alteration (possibly the case of the set of structures within the Arenal graben and to the west of Area A2).

The good correlation between gravity highs and magnetic lows is very suggestive in Areas A2, A0, and A1; for example, with its pesudo-gravity map it confirms the likelihood that the source of the anomalies are the same in Area A1. Although this kind of relationship needs to be evaluated together with other methods, it is suggested that the coincidence of thermal alteration zones with greater density zones can be solved by densification, which comes along with the destruction of magnetic minerals.

Meidav and Tonani (1975) point out in the Imperial Valley of California that local gravity anomalies are generally associated with metamorphism or densification of the sediments. Palmason (1975) states that structural methods may be used as indicators of geothermal alteration, considering the cause of the anomalies directly associated with the effect of the hydrothermal system on the host rock. He also groups the possible sources of gravity anomalies (for geothermal surveying) in; 1) hydrothermal alteration of reservoir rocks, 2) high proportion of intrusives, 3) structural features (faults, calderas, and basement structures).

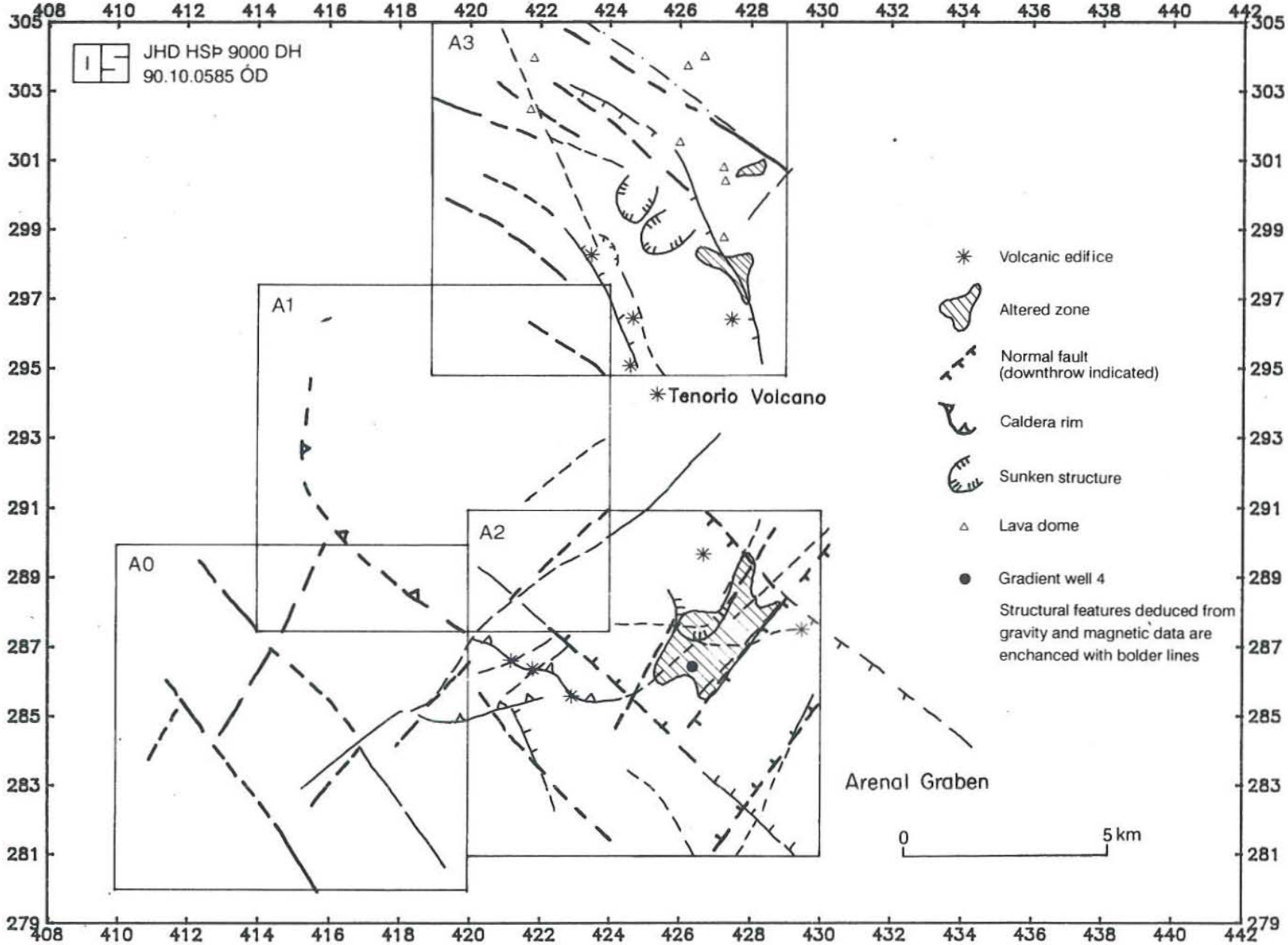

FIGURE 19: Structural synthesis map of the Tenorio area

In New Zealand positive gravity anomalies were considered to be due to rhyolitic domes and to hydrothermal alteration of the reservoir rocks (Macdonald and Muffler, 1972). It is important to be aware of the fact that the cause of these magnetic anomalies can also be due to the remains of fossil activity.

According to geochemical data, a northeast to southwest direction in Area A2 can be inferred for fluid circulation. Though it does not imply any kind of continuity, an impermeable barrier constraining the circulation and following the negative belt with the same direction could be postulated.

For the sake of this research, it is recommended to complete and improve the density of stations in Areas A3 and A2, in both of which the higher superficial manifestations occur. To complete a regional overview, analyzing the two volcanic systems, Miravalles and Tenorio, with the data available would be advisable. It is also recommended that this preliminary interpretation should be verified with other methods, and an integral interpretation made to be used as a guide for other exploration activities.

ACKNOWLEDGEMENTS

I would like to express my gratitude to Freyr Thorarinsson whose stimulating and unselfish guidance throughout this training has made this research possible. And to all the staff at Orkustofnun, especially director Ingvar Birgir Fridleifsson and subdirector Ludvik S. Georgsson from the United Nation University for their efforts during the Geothermal Training Programme, and to Marcia Kjartansson for her careful and patient correcting of the report.

Lastly, I thank the ICE and the representatives of the Geothermal division who gave me the opportunity for geothermal training in Iceland.

REFERENCES

Davis, J. C., 1986: Statistical and data analysis in geology. John Wiley and Sons, N.Y., 646 pp.

ICE, 1989: Geothermal pre-feasibility reconnaissence studies in the Costa Rican republic; II stage, pre-feseability study of the Tenorio area. Synthesis report, I.C.E., San José, Costa Rica (in Spanish).

LaFehr, T. R., 1965: The estimation of the total amount of anomalous mass by Gauss's theorem. J. Geophys. Res., 70, 1911-1919.

McDonald, W. J. P. and Muffler, L. J. P., 1972: Recent geophysical exploration of the Kawerau geothermal field, North Island, New Zealand. New Zealand Jour. Geol. and Geoph., 15, 303.

Meidav, T. and Tonani, F., 1975: A critique to geothermal exploration techniques. 2nd U.N. Symp. on the Development and Use of Geothermal Resources, San Franc., Proceedings, 1143-1154.

Palmason, G., 1975: Geophysical methods in geothermal exploration. 2nd U.N. Symp. on the Development and Use of Geothermal Resources, San Franc., Proceedings, 1175-1184.

Parasnis, D.S., 1972: Principles of applied geophysics. Chapman and Hall Ltd, London, 214 pp.

Thorarinsson, F. and Magnusson, S.G., 1989: STRIKE, version 4.0, gravity and magnetic data management and processing routines. Report and programme (unpublished), 65 pp.

Thorarinsson, F. and Magnusson, S.G., 1990: Bouguer density determination by fractal analysis. Geophysics, 55, 932-935.

Thorarinsson, F., Magnusson, S.G. and Björnsson, A., 1988: Directional spectral analysis and filtering of geophysical maps. Geophysics, vol 53, 1587-1591.

Torge, W., 1989: Gravimetry. Walter de Gruyter & Co., Berlin, 465 pp.